INTERNATIONAL JOURNAL FOR NUMERICAL METHODS IN FLUIDS
Int. J. Numer. Meth. Fluids 2008; **58**:27–55
Published online 7 January 2008 in Wiley InterScience (www.interscience.wiley.com). DOI: 10.1002/fld.1705

An anisothermal, compressible, piezoviscous model for journal-bearing lubrication

P. C. Bollada and T. N. Phillips*, †

School of Mathematics, Cardiff University, Senghennydd Road, Cardiff CF24 4AG, U.K.

SUMMARY

Compressibility plays a significant role in the load-bearing capacity of a journal bearing. This paper offers more realistic modelling of the lubricant than presented in an earlier paper (*Int. J. Numer. Meth. Fluids* 2007; **55**(11):1091–1120) by including variable sound speed, piezoviscosity and both temperature and shear thinning. The load-bearing capacity of the journal bearing is sensitive to all of these attributes of the model, but piezoviscosity is found to be the most significant. The equations of motion are adapted to a moving frame to explore the stability of the journal in a more dynamic setting and it is found that a free journal using this model will spiral outward exhibiting half speed whirl. The model is discretized in 2D, semi-implicitly in time and using the spectral element method in space. Numerical results are presented that highlight the contributions of the different elements in the model to journal stability. Copyright © 2008 John Wiley & Sons, Ltd.

Received 26 July 2007; Revised 31 October 2007; Accepted 2 November 2007

KEY WORDS: journal bearing; compressible fluid; spectral elements; piezoviscous fluid; anisothermal fluid; Tait equation of state

1. INTRODUCTION

In [1] the load-bearing capacity of a compressible Navier–Stokes fluid was explored and it was found that setting the speed of sound, c, to typical values found in a lubricant vastly improved the load-bearing capacity of an otherwise Newtonian incompressible fluid. This paper presents a model of a fluid that is compressible, anisothermal, shear thinning and piezoviscous. We use, respectively, the modified Tait equation of state (originated in [2]), Arrhenius, Cross and Barus law to model the fluid (see [3]). These modifications have an impact on the model by two means. First, the equation of state for pressure involves temperature as well as density and secondly,

*Correspondence to: T. N. Phillips, School of Mathematics, Cardiff University, Senghennydd Road, Cardiff CF24 4AG, U.K.
†E-mail: phillipstn@cf.ac.uk

Contract/grant sponsor: Engineering and Physical Sciences Research Council; contract/grant number: EP/C513037

temperature/pressure dependency of the viscosity coefficient in the momentum equations. By making reasonable assumptions on the model, namely, low volume expansion dependency on temperature, it is found that the direct effect of temperature in the equation of state on the momentum equations is negligible, although the isothermal Tait equation still has significant impact. The most significant impact comes from the pressure–temperature dependency of viscosity. We verify the conclusion in [4] that piezoviscous effects dominate at high eccentricities where wide ranges of pressure exist.

The coupling between the energy and momentum equations is governed by the constant, β, in the Arrhenius law. The value for β used in [5] is four times higher than the highest value used here, which is taken from [4] (other parameters being commensurate apart from viscosity, which is three orders of magnitude *less*). Since viscosity decreases with increased temperature and increases with increased pressure we expect, by setting the viscosity at room temperature and pressure equal to atmospheric pressure, that load-bearing capacity will be reduced by the temperature component and increased by the pressure dependency. The computation for the Arrhenius law becomes unstable for higher values of c, e.g. for $\beta=10$, as in [4], the simulation breaks down for $c=1500\,\mathrm{m\,s^{-1}}$ but is successful for $c=1250\,\mathrm{m\,s^{-1}}$ with the other parameter values remaining the same. This implies that compressibility has a stabilizing role in the simulation.

In previous work on the journal-bearing problem [6–9], it was assumed that the lubricant was incompressible. Bollada and Phillips [1] introduced compressibility using a linear isothermal equation of state. Here we introduce a nonlinear equation of state in the form of a modified Tait equation. In a centenary review of the Tait equation, Dymond and Malhotra [10] explore the relevance and form of the equation from its inception to modern day validity. It is, however, the modification due to Kirkwood and Bethe [11] that we adopt here in line with [12, 13] and also in Keshtiban *et al.* [14], where the authors investigate features of a compressible Oldroyd B fluid at various Mach numbers and compressibility within a finite element scheme. The treatment of pressure in these papers is different from to that presented here, where we replace the pressure variable by a function of density and temperature. It would then be convenient if density/viscosity relations were available. However, we have not been able to find many references regarding density-dependent viscosity and have hence adopted pressure-dependent relations, which in turn are related to density via an equation of state. The fact that one of the simplest models for viscosity derived from statistical mechanics is the compressible Navier–Stokes, which effectively sets viscosity proportional to density (see [15, 16]), suggests that density/temperature-dependent viscosity relations may be more fundamental than pressure/temperature dependency.

The Tait equation of state reduces to the linear equation of state when an index, m, is set to unity and has the effect of increasing the speed of sound, c, with density when $m>1$. On the basis of the results of [1], an increase in c reduces the load-bearing capacity of the journal bearing. However, we find that the use of the Tait equation has only a marginal effect on the dynamics, as might be expected for near incompressible fluids. However, compressibility still has a noticeable effect at realistic values for the speed of sound and begins to have quite significant effects for values of the speed of sound approaching 70% of its true value in oil. This strongly suggests that modelling of the gaseous phase (cavitation) should include some modelling of the speed of sound (see [17], for example) where the speed of sound drops to a level below that of the liquid *and* gas phase within the mixed phase region.

It was found in [1] that it was convenient to work with a kinematic extra-stress tensor, $\mathbf{T}$, rather than with the dynamic extra-stress tensor, $\mathbf{S}\equiv\rho\mathbf{T}$, where ρ is density, since, together with the use of constant kinematic viscosity, the coupled mass and momentum equations were largely

DOI: 10.1002/fld

linear. Constant kinematic viscosity is a feature of simple models produced from kinetic theory, e.g. Woods [15]. There are unavoidable nonlinearites associated with any realistic temperature-dependent model within the energy equation, but the compressibility of the model introduces further complications. Even when one assumes a constant Fourier heat conduction coefficient, κ, and heat capacity, C_V, the diffusion term remains nonlinear because of its coupling to a variable density. Just as the equation of state introduces negligible terms into the momentum equations, it also introduces extra-negligible terms into the energy equation. We revise the model by discarding these negligible terms.

The thermodynamic equations of state and internal energy are not independent. For an equation of state dependent on temperature (including isothermal) one cannot choose internal energy proportional to temperature. We show for an equation of state linear in temperature, however, that the necessary modification to the energy equation neatly cancels with the isotropic term, $-p\nabla\cdot\mathbf{u}$ ($\equiv -p\mathbf{I}:\nabla\mathbf{u}$), in the viscous heating contribution. This implies that the viscous heating term, $\mathbf{S}:\nabla\mathbf{u}$, where $\mathbf{S}$ is the extra-stress tensor together, with the assumption $e=C_V\Theta$ routinely adopted in the incompressible model, is effectively unaltered in the compressible case.

Finally, we generalize the investigation in [1] to include a journal moving within the bearing such that its centre of mass prescribes a circle with constant angular velocity, ω_{CM}, about the centre of the bearing. To investigate this we adopt a moving frame of reference with a rotating basis, which has the advantage of modifying the equations only to the extent of introducing the pseudo-forces—Coriolis and centrifugal. We demonstrate that as ω_{CM} approaches half the spin of the journal about its own centre, ω, the azimuthal force reduces to zero. At this critical value of ω_{CM} the direction of the force on the journal can be either inwards or outwards. An inward value suggests that the journal will move in towards the centre and conversely, as found here, an outward radial value indicates that the journal will spiral out. This suggests that the journal as modelled here is unstable and, unless its centre of mass motion is inhibited by a uni-directional load, the journal is predicted to fail.

2. GOVERNING EQUATIONS

2.1. Conservation equations

The conservation of momentum, or equation of motion, for a fluid is

$$\rho\frac{\mathrm{D}\mathbf{u}}{\mathrm{D}t}=-\nabla p+\nabla\cdot\mathbf{S} \tag{1}$$

where ρ is density, p is pressure, $\mathbf{u}$ is velocity and $\mathbf{S}$ is the extra-stress tensor. The extra-stress tensor for a compressible viscous fluid is given by

$$\mathbf{S}=\eta_1(\nabla\mathbf{u}+\nabla\mathbf{u}^{\mathrm{T}})+\eta_2(\nabla\cdot\mathbf{u})\mathbf{I} \tag{2}$$

where η_1 is the dynamic coefficient of viscosity (shear) and η_2 is the second coefficient of viscosity (dilatational). The quantity $\frac{2}{3}\eta_1+\eta_2$ is known as the bulk viscosity [18]. The bulk viscosity is relevant only in situations where the density is changing. Thus, it plays a role in attenuating sound waves in fluids and may be estimated from the magnitude of the attenuation.

DOI: 10.1002/fld

The conservation of mass, or equation of continuity, is expressed as

$$\frac{\mathrm{D}\rho}{\mathrm{D}t} = -\rho \nabla \cdot \mathbf{u} \tag{3}$$

The second viscosity coefficient is typically set to $\eta_2 = -\frac{2}{3}\eta_1$, which means that the bulk viscosity is zero and ensures that $\mathrm{tr}(\mathbf{S}) = 0$. This is known as Stokes' hypothesis.

The conservation of energy equation has the general mathematical form

$$\rho \frac{\mathrm{D}e}{\mathrm{D}t} = -p \nabla \cdot \mathbf{u} + \mathbf{S} : \nabla \mathbf{u} - \nabla \cdot \mathbf{h} \tag{4}$$

where e is the internal energy per unit mass and $\mathbf{h}$ is the heat flow vector.

3. EQUATION OF STATE

We consider the following equations of state:

- Linear model:

$$p = c_0^2(\rho - \rho_0) + p_0 \tag{5}$$

  where c_0 is the speed of sound, ρ_0 is a reference density and p_0 is atmospheric pressure.
- Modified Tait equation:

$$p - p_0 = c_0^2 \frac{\rho_0}{m} \left[\left(\frac{\rho}{\rho_0} \right)^m - 1 \right] \tag{6}$$

  where the constants are defined as in the linear model with the index m a free parameter depending on the fluid and typically set to $m = 4$ for lubricants and $m = 1$ to recover the linear model or ideal gas, explored in [1].
- Houpert equation [19, 20]:

$$p - p_0 = c_0^2 \frac{\rho - \rho_0}{1 - B(\rho/\rho_0 - 1)} \tag{7}$$

  where B is a free parameter determined by the experiment. We demonstrate that this model differs very little from the Tait equation for a large range of pressure for a typical lubricant (see Figure 1).
- Linear anisothermal model:

$$p = g(\rho) \left(1 + \alpha \frac{\Theta}{\Theta_0} \right) \tag{8}$$

  where $\Theta \equiv \tilde{\Theta} - \Theta_0$, $\tilde{\Theta}$ is the absolute temperature and Θ_0 a reference temperature. The parameter α is related to the expansion of the fluid at $\Theta = 0$. A value of $\alpha = 0$ corresponds to isothermal flow and $\alpha = 1$ to an ideal gas equation.

for some isothermal model $p = g(\rho)$, i.e. we convert each of the equations of state (5)–(7) to its anisothermal equivalent by multiplying by $(1 + \alpha(\Theta/\Theta_0))$.

DOI: 10.1002/fld

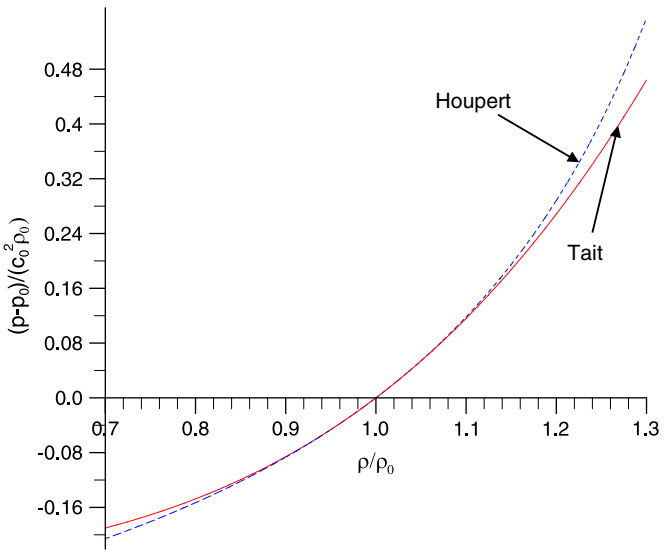

Figure 1. The (scaled) pressure using the Tait equation ($m=4$) and Houpert (dashed) ($B=1.53$). The two models are in good agreement for changes in density $\rho \in [\rho_0 \pm \rho_0/10]$, e.g. for eccentricity ratio, $\varepsilon = 0.8$ we find $\rho/\rho_0 \in [0.97, 1.05]$.

3.1. *Viscosity relations*

The viscosity relations explored are:

- Constant kinematic viscosity:

$$\eta = \mu\rho \tag{9}$$

  which leads to the compressible Newtonian model explored in [1]
- Barus equation:

$$\eta = \eta_0 \exp(A[p - p_0]) = \eta_0 \exp\left(\gamma \frac{p - p_0}{p_0}\right) \tag{10}$$

  for some free parameter A, or γ being a dimensionless equivalent.
- Shear thinning—Cross model:

$$\eta = \eta_\infty + \frac{\eta_0 - \eta_\infty}{1 + C(k\dot{\gamma})^N} \tag{11a}$$

  where C is a free dimensionless parameter and k is, in general, a function of pressure and temperature via, for example, the Barus and Arrhenius equations (13b). The strain rate, $\dot{\gamma}$, is defined as

$$\dot{\gamma} \equiv \sqrt{\nabla\mathbf{u} : \nabla\mathbf{u} + \nabla\mathbf{u} : \nabla\mathbf{u}^{\mathrm{T}}} \tag{11b}$$

DOI: 10.1002/fld

- Temperature thinning—Arrhenius Law:

$$\eta = \eta_0 \exp\left(\frac{-\beta\Theta/\Theta_0}{1+\Theta/\Theta_0}\right) \tag{12}$$

for free dimensionless parameter, β.

- Combined Tait–Arrhenius–Barus–Cross:

$$\eta = \left[\eta_\infty + \frac{\eta_0 - \eta_\infty}{1+C(k\dot{\gamma})^N}\right] \times k(\rho, \Theta) \tag{13a}$$

and

$$k \equiv k(\rho, T) = \exp\left(\gamma \frac{p-p_0}{p_0}\right) \times \left(\frac{-\beta\Theta/\Theta_0}{1+\Theta/\Theta_0}\right) \tag{13b}$$

where the Tait law is modified to

$$p = p_0 + c_0^2 \frac{\rho_0}{m}\left[\left(\frac{\rho}{\rho_0}\right)^m - 1\right] \times \left(1+\alpha\frac{\Theta}{\Theta_0}\right) \tag{13c}$$

The term $\alpha\Theta/\Theta_0$ in (13c) has a negligible and opposing effect on viscosity to the Arrhenius term and hence we write express as

$$k \equiv \exp\left(\frac{\gamma c_0^2 \rho_0}{p_0 m}[(\rho/\rho_0)^m - 1]\right) \times \left(\frac{-\beta\Theta/\Theta_0}{1+\Theta/\Theta_0}\right) \tag{13d}$$

The parameter values are given in Tables I and II. The values for density, viscosity and journal-bearing dimensions are taken from [1, 21]; other constants are taken from [5].

Figure 1 shows a comparison of the speed of sound for the Tait equation and Houpert equation with constants $m=4$ and $B=1.53$, respectively, suggesting that the models are virtually interchangeable within a large range of density values.

3.2. The influence of the equation of state on the conservation equations

For flow where thermal effects are taken into account, we assume the existence of an equation of state:

$$p = p(\rho, \Theta)$$

Table I. The dimensionless parameters appearing in the constitutive relations, equations of state and viscosity laws.

Dimensionless parameter	Value
Bi	0.01
γ	2.1×10^{-3}
β	2
C	4.2×10^{-4}
α	4×10^{-4}
m	4

DOI: 10.1002/fld

Table II. The dimensional parameter values in S.I. and scaled units.

Parameter	Value (S.I. units)	Value (scaled units)
R_B	$0.05\,\mathrm{m}$	1
ω	$500\,\mathrm{s}^{-1}$	1
ρ_0	$800\,\mathrm{kg\,m}^{-3}$	1
Θ_0	$300\,\mathrm{K}$	1
$R_B - R_J$	$5\times10^{-5}\,\mathrm{m}$	1×10^{-3}
c_0	$1500\,\mathrm{m\,s}^{-1}$	60
η_0	$5\times10^{-3}\,\mathrm{Pa\,s}$	1×10^{-5}
η_∞	$2.5\times10^{-3}\,\mathrm{Pa\,s}$	0.5×10^{-5}
C_V	$1.75\times10^{3}\,\mathrm{W\,kg}^{-1}\,\mathrm{K}^{-1}$	840
κ	$0.14\,\mathrm{W\,m}^{-1}\,\mathrm{K}^{-1}\,\mathrm{s}^{-1}$	1.344×10^{-4}
h	$5\times10^{-4}\,\mathrm{m}$	1×10^{-2}

where Θ is temperature. So that in general,

$$\nabla p = \frac{\partial p}{\partial \rho}\nabla\rho + \frac{\partial p}{\partial \Theta}\nabla\Theta$$

It is convenient to express viscosity in the forms

$$\eta_1(\rho,\Theta) = \mu(\rho,\Theta)\rho, \quad \eta_2(\rho,\Theta) = -\tfrac{2}{3}\mu(\rho,\Theta)\rho \tag{14}$$

where μ is the kinematic viscosity (chosen constant in [1]). Thus, we can rewrite (1) as

$$\frac{\mathrm{D}\mathbf{u}}{\mathrm{D}t} = -\frac{\partial p}{\partial \rho}\nabla q - \frac{1}{\rho}\frac{\partial p}{\partial \Theta}\nabla\Theta + \nabla\cdot\mathbf{T} + \nabla q\cdot\mathbf{T}$$

where the kinematic extra stress is defined

$$\mathbf{T} \equiv \mu(\nabla\mathbf{u} + \nabla\mathbf{u}^{\mathrm{T}}) - \tfrac{2}{3}\mu(\nabla\cdot\mathbf{u})\mathbf{I} \equiv \frac{1}{\rho}\mathbf{S} \tag{15}$$

and we define the log density $q \equiv \ln\rho$.

We choose the equation of state, (8), which is linear in temperature Θ. Using the thermodynamic law,

$$\mathrm{d}U = \tilde{\Theta}\,\mathrm{d}S - p\,\mathrm{d}V \tag{16}$$

where S is entropy, and noting that the linear equation of state can be expressed in terms of a specific volume, $V = 1/\rho$:

$$p = g(\rho)\frac{\alpha\tilde{\Theta}}{\Theta_0} + g(\rho)(1-\alpha) = g(1/V)\frac{\alpha\tilde{\Theta}}{\Theta_0} + g(1/V)(1-\alpha)$$

Then the condition on the internal energy is

$$\left(\frac{\partial e}{\partial V}\right)_{\tilde{\Theta}} = \tilde{\Theta}\left(\frac{\partial p}{\partial \tilde{\Theta}}\right)_V - p$$

DOI: 10.1002/fld

This implies

$$e=(1-\alpha)\int g(1/V)\,\mathrm{d}V+f(\tilde{\Theta})$$

$$=-(1-\alpha)\int\frac{g(\rho)}{\rho^2}\,\mathrm{d}\rho+f(\tilde{\Theta})$$

where f is arbitrary. We choose the simplest option without violating (16) and express the internal energy as

$$e=-(1-\alpha)\int\frac{g(\rho)}{\rho^2}\,\mathrm{d}\rho+C_V\tilde{\Theta} \tag{17}$$

This implies

$$\frac{\mathrm{D}e}{\mathrm{D}t}=-(1-\alpha)\frac{g(\rho)}{\rho^2}\frac{\mathrm{D}\rho}{\mathrm{D}t}+C_V\frac{\mathrm{D}\tilde{\Theta}}{\mathrm{D}t}$$

$$=(1-\alpha)\frac{g(\rho)}{\rho}\nabla\cdot\mathbf{u}+C_V\frac{\mathrm{D}\tilde{\Theta}}{\mathrm{D}t}$$

With Fourier's law

$$\mathbf{h}=-\kappa\nabla\Theta \tag{18}$$

we now have sufficient information to close the equations, giving

$$\frac{\mathrm{D}\mathbf{u}}{\mathrm{D}t}=-g'(\rho)\left(1+\frac{\alpha\Theta}{\Theta_0}\right)\nabla q-\frac{\alpha g(\rho)}{\rho\Theta_0}\nabla\Theta+\nabla\cdot\mathbf{T}+\nabla q\cdot\mathbf{T}$$

$$=-g'(\rho)\nabla q+\nabla\cdot\mathbf{T}-\frac{\alpha g(\rho)}{\rho\Theta_0}\nabla\Theta+\nabla q\cdot\left(\mathbf{T}-\alpha g'(\rho)\frac{\Theta}{\Theta_0}\mathbf{1}\right)$$

The continuity equation can be expressed using q as

$$\frac{\mathrm{D}q}{\mathrm{D}t}=-\nabla\cdot\mathbf{u} \tag{19}$$

and finally the energy equation is

$$C_V\frac{\mathrm{D}\Theta}{\mathrm{D}t}=(1-\alpha)\frac{g(\rho)}{\rho}\nabla\cdot\mathbf{u}+\exp(-q)\kappa\nabla^2\Theta+\left(\mathbf{T}-\frac{g(\rho)}{\rho}\left(\frac{\alpha\Theta}{\Theta_0}+1\right)\mathbf{I}\right):\nabla\mathbf{u}$$

$$=-\frac{g(\rho)}{\rho}\alpha\left(1+\frac{\Theta}{\Theta_0}\right)\nabla\cdot\mathbf{u}+\frac{\kappa}{\rho}\nabla^2\Theta+\mathbf{T}:\nabla\mathbf{u}$$

where we note that the cancellation comes about from $\nabla\cdot\mathbf{u}\equiv\mathbf{I}:\nabla\mathbf{u}$ and the implication that the adoption of $e=C_V\Theta$ is closely connected with the use of the extra stress in the viscous heating term $\mathbf{T}:\nabla\mathbf{u}$.

DOI: 10.1002/fld

We find that once integrated there are some negligible terms in the momentum equations. With these terms removed and using the Tait equation for $g(\rho)$ we are left with momentum conservation:

$$\frac{\mathrm{D}\mathbf{u}}{\mathrm{D}t} = -c_0^2 \left(\frac{\rho}{\rho_0}\right)^{m-1} \nabla q + \nabla \cdot \mathbf{T} \tag{20}$$

where the kinematic stress tensor, $\mathbf{T}$, is given by (15), mass conservation is given by (19) and the conservation of energy is

$$C_V \frac{\mathrm{D}\Theta}{\mathrm{D}t} = \exp(-q)\kappa \nabla^2 \Theta + \mathbf{T} : \nabla \mathbf{u} - \frac{g(\rho)}{\rho} \alpha \left(1 + \frac{\Theta}{\Theta_0}\right) \nabla \cdot \mathbf{u} \tag{21}$$

where the last term, which is of order $c_0^2 \alpha \approx 10^2$, is significant:

$$\frac{g(\rho)}{\rho} = \frac{c_0^2 \rho_0}{m\rho} \left[\left(\frac{\rho}{\rho_0}\right)^m - 1\right] + \frac{p_0}{\rho} \approx \frac{c_0^2 \rho_0}{m\rho} \left[\left(\frac{\rho}{\rho_0}\right)^m - 1\right]$$

4. THE STATICALLY LOADED JOURNAL-BEARING PROBLEM

Consider the two-dimensional geometry shown schematically in Figure 2. The journal of radius R_J rotates with a predetermined constant angular velocity ω about its own centre. The journal's motion is lubricated by a fluid lubricant contained within a stationary bearing of radius R_B. Both the journal and the bearing are assumed to be of infinite extent in the axial z-direction. The time-dependent eccentricity of the system is denoted by e, with the eccentricity ratio defined by $\varepsilon = e/(R_B - R_J)$, $0 \leqslant \varepsilon \leqslant 1$. Therefore, when $\varepsilon = 1$ the journal is in contact with the bearing and when $\varepsilon = 0$ the journal and bearing are concentric.

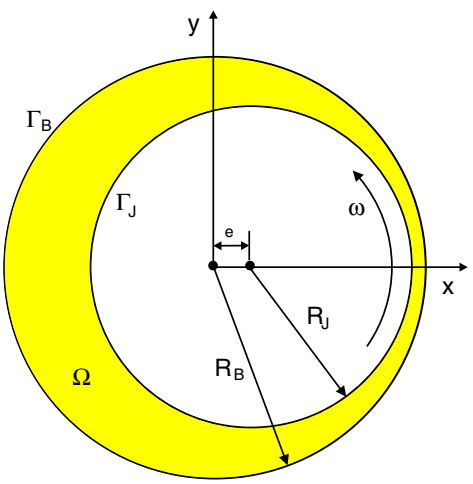

Figure 2. Schematic picture of a journal bearing with the difference in radius exaggerated for clarity.

DOI: 10.1002/fld

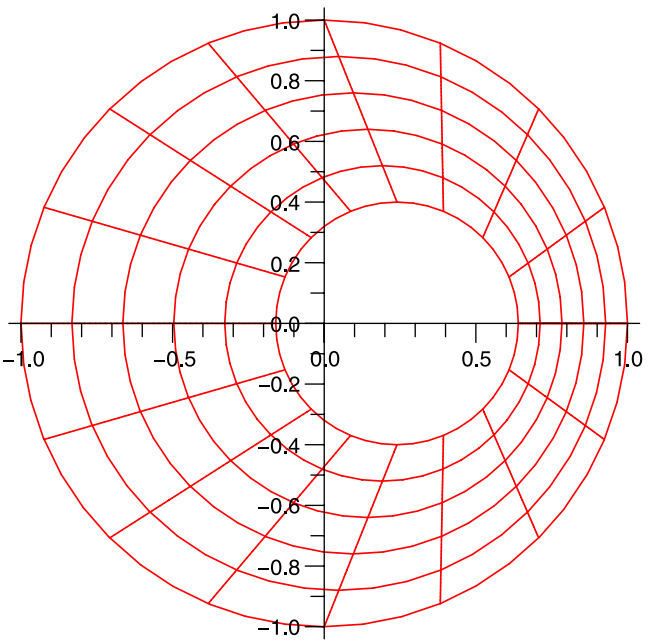

Figure 3. A coordinate system for the journal bearing. This coordinate system has the feature that constant r describes a circle and radial lines meet at the point $(\varepsilon, 0)$.

The lubricant satisfies the governing equations (15), (19)–(21) which are solved subject to specified boundary and initial conditions. These are, respectively,

$$\mathbf{u}(\mathbf{x},t)=\mathbf{V}(t) \text{ with } \mathbf{x}\in\Gamma_J, \quad \mathbf{u}(\mathbf{x},t)=\mathbf{0} \text{ with } \mathbf{x}\in\Gamma_B \tag{22}$$

$$\Theta(\mathbf{x},t)=\Theta_J \text{ with } \mathbf{x}\in\Gamma_J, \quad \nabla\Theta(\mathbf{x},t)\cdot\mathbf{n}=-\frac{\mathrm{Bi}}{h}\Theta(\mathbf{x},t) \text{ with } \mathbf{x}\in\Gamma_B \tag{23}$$

$$\mathbf{u}(\mathbf{x},t=0)=\mathbf{u}_0(\mathbf{x}), \quad \Theta(\mathbf{x},t=0)=\Theta_0(\mathbf{x}) \tag{24}$$

where Γ_J and Γ_B denote the boundaries of the journal and bearing, respectively. The boundary condition on the temperature is known as the Biot–Robin condition, where h is a length scale associated with the problem and Bi is associated with the thermal conductivity of the bearing. See Li *et al.* [5] for an extended discussion on this issue.

We consider the following coordinate system in the journal-bearing configuration (see Figure 3)

$$\begin{aligned} x &= r\cos\theta+\varepsilon(1-r)\\ y &= r\sin\theta \end{aligned} \tag{25}$$

for $r\in[R_J,1]$ and $\theta\in[0,2\pi]$, where the radial distance has been scaled by R_B. The eccentricity ratio, in terms of the scaled radius, is now defined by

$$\varepsilon=\frac{e}{1-R_J}$$

DOI: 10.1002/fld

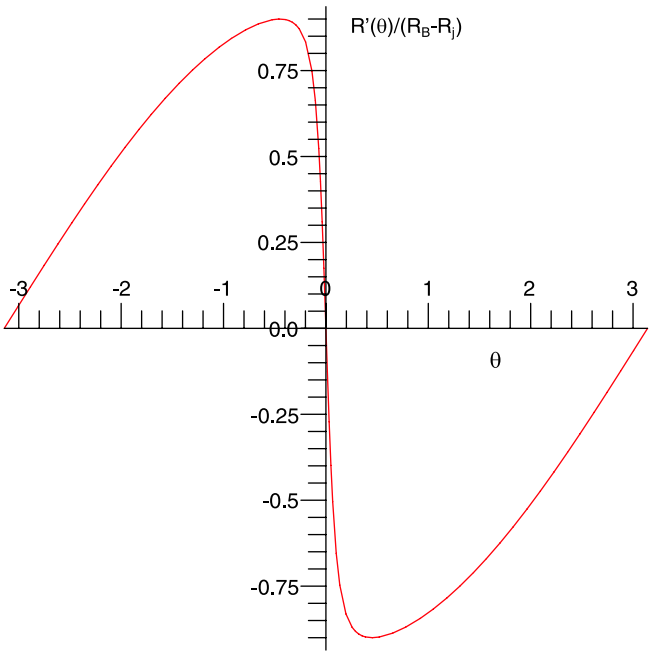

Figure 4. Plot of the rate of change of gap in the journal-bearing $\partial R/\partial\theta$ divided by the difference in radii $1-R_J=10^{-4}$. The slope is thus very small suggesting that streamlines converge only slightly.

The distance between the journal and the bearing (along a radial spoke) is given by

$$R\equiv(1-R_J)\sqrt{(1-2\varepsilon\cos\theta+\varepsilon^2)}$$

with slope (see Figure 4)

$$\frac{\partial R}{\partial\theta}=\frac{(1-R_J)\varepsilon\sin\theta}{\sqrt{(1-2\varepsilon\cos\theta+\varepsilon^2)}}$$

and because $1-R_J\ll 1$ the slope is small and we expect the stream lines to be near parallel. Since we are using a (generalized) Newtonian model, this suggests that normal forces are negligible compared with shear forces (there are no normal forces for a Newtonian fluid in simple shear flow). This means that even though there can be a large contraction of the flow around the journal bearing, the transition from large to small gap is gradual as compared with, say, an abrupt 4:1 contraction in channel flow.

The derivatives associated with the transformation are related through

$$\begin{bmatrix}\dfrac{\partial}{\partial r}\\[2ex]\dfrac{\partial}{\partial\theta}\end{bmatrix}=\begin{bmatrix}\cos\theta-\varepsilon & \sin\theta\\ -r\sin\theta & r\cos\theta\end{bmatrix}\begin{bmatrix}\dfrac{\partial}{\partial x}\\[2ex]\dfrac{\partial}{\partial y}\end{bmatrix}\tag{26}$$

DOI: 10.1002/fld

so that

$$\begin{bmatrix} \dfrac{\partial}{\partial x} \\ \dfrac{\partial}{\partial y} \end{bmatrix} = \begin{bmatrix} r\cos\theta/J_1 & -(\sin\theta)/J_1 \\ r\sin\theta/J_1 & (\cos\theta-\varepsilon)/J_1 \end{bmatrix} \begin{bmatrix} \dfrac{\partial}{\partial r} \\ \dfrac{\partial}{\partial \theta} \end{bmatrix} \tag{27}$$

where $J_1 \equiv r(1-\varepsilon\cos\theta)$.

5. THE WEAK FORMULATION

Let Ω denote the region between the journal and bearing. At each time step, a solution is sought in the following spaces:

$$\mathbf{W} = \{\mathbf{w} : w^a \in H^1(\Omega), a \in [1,2], \mathbf{w} = \mathbf{V} \text{ on } \Gamma_J, \mathbf{w} = \mathbf{0} \text{ on } \Gamma_B\}$$

$$P = H^1(\Omega)$$

$$V = \{H^1(\Omega),\ v = 0 \text{ on } \partial\Omega_J\}$$

$$\mathbf{R} = [H^1(\Omega)]_s^4$$

where the extra-stress space $\mathbf{R}$ is the space of symmetric 2×2 tensors whose components belong to $H^1(\Omega)$, and Γ_J and Γ_B are the boundaries of the journal and bearing, respectively. We also define the test space, $\mathbf{W}_0$, for the velocity:

$$\mathbf{W}_0 = \{\mathbf{w} : w^a \in H^1(\Omega), a \in [1,2], \mathbf{w} = \mathbf{0} \text{ on } \Gamma_J \text{ and } \Gamma_B\}$$

The weak formulation is then: find $\mathbf{u} \in \mathbf{W}$, $q \in P$, $\mathbf{T} \in \mathbf{R}$ and $\Theta \in V$, such that

$$\int_\Omega \frac{\mathbf{u}-\mathbf{u}^n}{\Delta t}\cdot\mathbf{w} - \int_\Omega c^2 q \nabla\cdot\mathbf{w} + \int_\Omega \mathbf{T} : \nabla\mathbf{w} = 0 \quad \forall \mathbf{w} \in \mathbf{W}_0 \tag{28}$$

$$\int_\Omega \left(\frac{q-q^n}{\Delta t} + \nabla\cdot\mathbf{u}\right) w = 0 \quad \forall w \in P \tag{29}$$

$$\int_\Omega \mathbf{T} : \mathbf{W} - \int_\Omega \mu\nabla\mathbf{u} : (\mathbf{W}+\mathbf{W}^{\mathrm{T}}) + \frac{2}{3}\int_\Omega \mu\nabla\cdot\mathbf{u}\,\mathrm{tr}(\mathbf{W}) = 0 \quad \forall \mathbf{W} \in \mathbf{R} \tag{30}$$

$$\begin{aligned} C_V \int_\Omega \left(\frac{\Theta-\Theta^n}{\Delta t}\right) v + \kappa \int_\Omega \exp(-q^n)\nabla\Theta\cdot\nabla v \\ = \kappa \int_{\partial\Omega_B} \exp(-q^n)\nabla\Theta^n\cdot\mathbf{n}v + \int_\Omega \mathbf{T}^n : \nabla\mathbf{u}^n v \\ - \int_\Omega \exp(-q^n) g^n \alpha \left(1 + \frac{\Theta^n}{\Theta_0}\right)\nabla\cdot\mathbf{u}^n v \quad \forall v \in V \end{aligned} \tag{31}$$

where $c^2 \equiv \partial p/\partial\rho$ and μ, v are functions of Θ, q and $\dot{\boldsymbol{\gamma}}$.

DOI: 10.1002/fld

For enhanced numerical stability, we treat $\exp(-q)\kappa\nabla^2\Theta$ semi-implicitly in the energy equation (31), and all other terms are treated explicitly. The boundary term is treated explicitly since its contribution is not symmetric when treated implicitly. This implies: Dirichlet boundary conditions for $\mathbf{u}$; no boundary conditions for q and $\mathbf{T}$; Dirichlet boundary conditions on Θ on the journal. We use the Biot–Robin condition on the bearing to control the heat flow out of the bearing:

$$\int_{\partial\Omega_B} \nabla\Theta\cdot\mathbf{n}v = -\int_{\partial\Omega_B} \frac{\mathrm{Bi}}{h}\Theta v$$

where Bi is a suitable Biot constant, and h is a characteristic length. On substitution into (31) we find

$$\begin{aligned} C_V\int_\Omega\left(\frac{\Theta-\Theta^n}{\Delta t}\right)v+\kappa\int_\Omega \exp(-q^n)\nabla\Theta\cdot\nabla v \\ =\frac{\kappa\,\mathrm{Bi}}{h}\int_{\partial\Omega_B}\exp(-q^n)\Theta^n v+\int_\Omega \mathbf{T}^n:\nabla\mathbf{u}^n v \\ -\int_\Omega \exp(-q^n)g^n\alpha\left(1+\frac{\Theta^n}{\Theta_0}\right)\nabla\cdot\mathbf{u}^n v \quad \forall v\in V \end{aligned} \tag{32}$$

6. SPECTRAL ELEMENT DISCRETIZATION

We refer the reader to [1] for much of the details regarding the discretization depicted in Figure 5. The results are summarized as follows. The conservation of momentum and mass produce the system for the velocity field, $\bar{u}^a\equiv u^a_{ij}$ and log density $\bar{q}\equiv q_{ij}$ at the GL points (i,j):

$$\bar{u}^a\cdot\bar{\bar{M}}^{ab}=\bar{v}^b \tag{33}$$

where

$$\bar{\bar{M}}^{ab}=\bar{\bar{A}}\delta^{ab}+[(\bar{\bar{C}}^c_T\cdot\bar{\bar{\mu}}\cdot\bar{\bar{A}}^{-1}\cdot\bar{\bar{C}}^c\delta^{ab}+\bar{\bar{C}}^b_T\cdot\bar{\bar{\mu}}\cdot\bar{\bar{A}}^{-1}\cdot\bar{\bar{C}}^a)+\bar{\bar{C}}^a_T\cdot(\bar{\bar{c}}^2\Delta t-\tfrac{2}{3}\bar{\bar{\mu}})\cdot\bar{\bar{A}}^{-1}\cdot\bar{\bar{C}}^b]\Delta t \tag{34}$$

and

$$\bar{v}^b\equiv(\bar{u}^b)^n\cdot\bar{\bar{A}}+\Delta t\bar{\bar{c}}^2\cdot\bar{q}^n\cdot\bar{\bar{C}}^b \tag{35}$$

The log density, q is given by

$$\bar{q}\cdot\bar{\bar{A}}+\Delta t\bar{u}^b\cdot\bar{\bar{C}}^b_T=\bar{q}^n\cdot\bar{\bar{A}} \tag{36}$$

The discretization of the conservation of energy gives an equation for temperature, $\bar{\Theta}\equiv\Theta_{ij}$

$$\bar{\Theta}\cdot\bar{\bar{N}}=\bar{\tau} \tag{37}$$

where

$$\bar{\bar{N}}=\bar{\bar{I}}-\Delta t\frac{\kappa}{C_V}\bar{\bar{C}}^a_T\cdot\bar{\bar{\kappa}}\cdot\bar{\bar{A}}^{-1}\cdot\bar{\bar{C}}^a\cdot\bar{\bar{A}}^{-1}$$

$$\bar{\tau}=\bar{\Theta}^n+\frac{\Delta t}{C_V}\bar{\phi}\cdot\bar{\bar{A}}^{-1}$$

DOI: 10.1002/fld

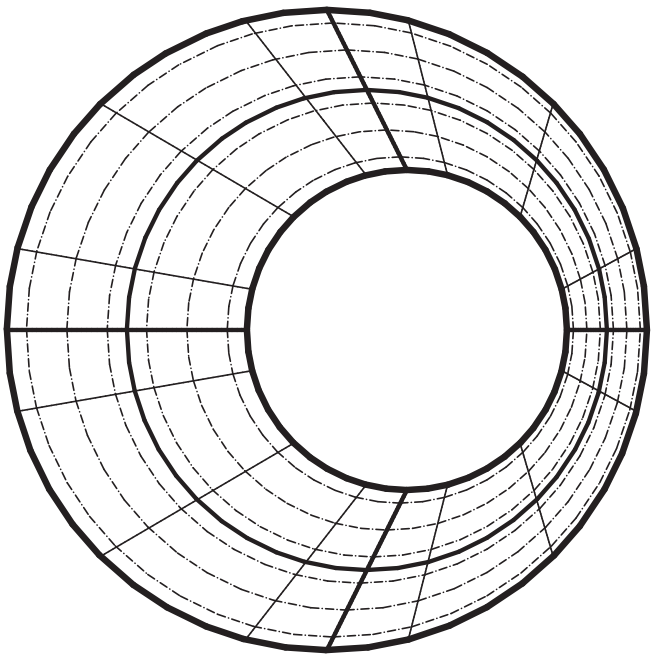

Figure 5. The discretization of the physical domain into four elements in the azimuthal direction and two in the radial direction. The thick lines outline the 4×2 spectral elements and the dashed lines meet at Gauss–Lobatto points for order $N=4$ in both directions.

We also require a boundary integral due to the Biot–Robin condition. For elements next to the bearing ($\alpha=\hat{\alpha}$):

$$\begin{aligned}\int_{\partial\Omega}\Theta v &= \int_0^{2\pi}\Theta(\phi)v\,\mathrm{d}\phi\\ &= \delta_{Nk}\sum_{\beta=0}^{\hat{\beta}}\int_{-1}^{1}\Theta(\xi_N,\zeta)h_l(\zeta)\frac{\partial\phi}{\partial\zeta}\,\mathrm{d}\zeta\\ &= \delta_{Nk}\sum_{\beta=0}^{\hat{\beta}}\Theta_{N,l}^{\hat{\alpha},\beta}\left(\frac{\partial\phi}{\partial\zeta}\right)_l^{\beta}\lambda_l\\ &= \sum_{\beta=0}^{\hat{\beta}}\Theta_{ij}^{\hat{\alpha},\beta}\delta_{Ni}\delta_{jl}\delta_{Nk}\left(\frac{\partial\phi}{\partial\zeta}\right)_l^{\beta}\lambda_l\\ &= \sum_{\beta=0}^{\hat{\beta}}\Theta_{ij}^{\hat{\alpha},\beta}B_{ijkl}^{\beta}\end{aligned}$$

DOI: 10.1002/fld

where the local matrix

$$B^{\beta}_{ijkl} \equiv \delta_{Ni}\delta_{jl}\delta_{Nk}\left(\frac{\partial\phi}{\partial\zeta}\right)^{\beta}_{l}\lambda_l$$

Other matrices are defined:

$$(\bar{u}^a)_{ij} \equiv u^a_{ij}, \quad (\bar{A})_{ijkl} \equiv A_{ijkl}, \quad (\bar{T}^{ab})_{ij} \equiv T^{ab}_{ij}, \quad (\bar{\bar{C}}^b)_{ijkl} \equiv C^b_{ijkl}, \quad (\bar{q})_{ij} \equiv q_{ij}$$

$$(\bar{\bar{\mu}})_{ijkl} \equiv \mu_{kl}\delta_{ik}\delta_{jl}, \quad (\bar{\bar{c}}^2)_{ijkl} \equiv c^2_{kl}\delta_{ik}\delta_{jl}, \quad (\bar{\bar{\kappa}})_{kl} \equiv (\kappa/\rho_{kl})\delta_{ik}\delta_{jl}, \quad (\bar{\bar{C}}^a_T)_{ijkl} \equiv C^a_{klij}$$

$$\bar{\phi}_{kl} \equiv \bar{T}^{ab}_{kl}(\bar{u}^a \cdot \bar{\bar{C}}^b_T)_{kl} - \frac{g(\rho_{kl})}{\rho_{kl}}\alpha(1+\Theta_{kl})(\bar{u}^a \cdot \bar{\bar{C}}^a_T)_{kl} - \frac{\kappa\,\mathrm{Bi}}{h}\exp(-q)\bar{\Theta}^n \cdot \bar{\bar{B}}_{kl}$$

The array $\bar{\bar{A}}$ contains weights, λ_i, and the Jacobian, J_{ij}, of the spectral element mappings; $\bar{\bar{C}}_b \equiv \bar{C}^{ijkl}_b$ is the discretization associated with the gradient operator, ∇:

$$\begin{aligned}
\bar{A}_{ijkl} &\equiv \int_S J(\xi,\zeta)h_i(\xi)h_j(\zeta)h_k(\xi)h_l(\zeta) = J_{ij}\lambda_i\lambda_j\delta_{ki}\delta_{lj} \quad \text{(no sum)} \\
\bar{C}^{ijkl}_b &\equiv \int_S Z^{cb}(\xi,\zeta)h_i(\xi)h_j(\zeta)[h_k(\xi)h_l(\zeta)]_{,c} = \lambda_i\lambda_j Z^{cb}_{ij}\begin{cases} D_{ik}\delta_{lj}, & c=1 \\ \delta_{ki}D_{jl}, & c=2 \end{cases}
\end{aligned} \tag{38}$$

Further information regarding differential operators, $D_{ij} \equiv h'_i(\xi_j)$, Z^{cb}_{ij} assembling global arrays from local arrays can be found in [1].

6.1. The force on the journal due to the fluid

The force, **F**, on the journal is given by

$$\mathbf{F} \equiv -\int_C \boldsymbol{\sigma}\cdot\mathbf{n}\,\mathrm{d}C \tag{39}$$

where C is the boundary of the journal, **n** is the unit outward normal to the boundary (radial direction) and $\boldsymbol{\sigma} \equiv -p\mathbf{I}+\mathbf{S}$ is the total or Cauchy stress. In two dimensions, this is conveniently expressed as

$$F^a = \int_C \sigma^{ab}\varepsilon^{bc}\,\mathrm{d}x^c \tag{40}$$

where ε^{bc} is the second-order alternating symbol. In fact, a good approximation to the force in this application is obtained by ignoring the extra stress, **S**, contribution altogether and expressed the components of force as

$$F^a = \int_C \sigma^{ab}\varepsilon^{bc}\,\mathrm{d}x^c = \int_C (S^{ab}-p\delta^{ab})\varepsilon^{bc}\,\mathrm{d}x^c \approx -\int_C p\varepsilon^{ab}\,\mathrm{d}x^b \tag{41}$$

Using Gaussian quadrature on the journal boundary this is (see [1])

$$F^a = \sum_j \lambda_j(-p(\rho_{0,j})\delta^{ab} + \rho_{0,j}T^{ab}_{0,j})\varepsilon^{bc}\left.\frac{\partial x^c}{\partial\zeta}\right|_{0,j}, \quad j \in [1, N(\beta+1)] \tag{42}$$

DOI: 10.1002/fld

Similarly, the resultant torque, Λ, on the journal is given by

$$\Lambda = R \int_C S^{ab} n^a \, \mathrm{d}x^b \tag{43}$$

7. THE EFFECT OF THE TAIT, BARUS, ARRHENIUS AND CROSS MODEL ON LOAD-BEARING CAPACITY

In an earlier paper [1], it was shown that the load-bearing capacity increases with viscosity; hence, we expect temperature thinning to decrease this capacity given the high operating temperatures within the journal bearing. We also expect shear thinning to reduce the load-bearing capacity as a result of reduction in the average viscosity. On the other hand, the use of the Barus law is predicted to increase the average viscosity. These models have been explored for incompressible fluids in a dynamically loaded setting, for example, in [5]. Here we explore these models together with the Tait equation to examine the similarities and differences that compressibility introduces.

Figure 6 shows the forces away from the narrow gap at eccentricity ratio $\varepsilon = 0.8$ for a range of combinations of the models and reference sound speed ($c_0 = 1000, 1250, 1500\,\mathrm{m\,s^{-1}}$) corresponding to respectively smaller values of F_x.[‡] The dimensions are scaled so that a unit of force/unit length corresponds to $\rho_0 R_J^3 \omega^2 = (800\,\mathrm{kg\,m^{-3}})(0.05\ \mathrm{m})^3(500\,\mathrm{s^{-1}})^2 = 25\,000\,\mathrm{N\,m^{-1}}$ and so the forces involved here are of the order of $10^6\,\mathrm{N\,m^{-1}}$ (this corrects an error in [1], where the forces shown are in the scaled units and not Newtons as indicated). The relation implies that force is proportional to density, to the cube of journal radius and square of angular velocity. The symbols—cross, box, circle and diamond—represent the compressible Newtonian, Barus, Barus + Arrhenius, Barus + Arrhenius + Cross models, respectively. The small and large symbols are constant sound speed and Tait equation, respectively. The scaling in the figure disguises the fact that all the results have a similar component of force in the y-direction, i.e. normal to the line joining the centres of the journal and bearing. In the x-direction, however, there is an appreciable difference between the constant kinematic viscosity (compressible Newtonian) and the other models.

These results show that modelling the equation of state with the Tait equation produces results varying only slightly from those with a linear equation of state. This observation is to be expected for a near incompressible fluid.

As a measure of stability in a fluid for the journal bearing, we define a stability measure: $\chi = -F_x/F_y$, for which we have stability when $\chi \to \infty$ and increasing instability for $\chi \leqslant 0$. Using this criterion there is little difference between the models: Barus, Barus + Arrhenius and Barus + Arrhenius + Cross, see Table III. In comparison, the constant kinematic viscosity model offers significantly less stability at these values.

The force on the journal is dominated by the pressure around the journal. Two sets of pressure profiles around the journal, with the narrow gap marked by vertical lines, are shown in Figure 7 showing pressures of the order of 500 Bar. The left-hand set are for the higher value of $c_0 = 60 R_J \omega = 1500\,\mathrm{m\,s^{-1}}$ and the right-hand set for $c_0 = 40 R_J \omega = 1000\,\mathrm{m\,s^{-1}}$. In the flow converging to the narrow gap the pressure is high and while leaving the narrow gap, it is low. The highest (and lowest) pressures are achieved with the Barus model with a Tait equation of state. These

[‡]Respectively, red, blue and green, in the electronic version.

DOI: 10.1002/fld

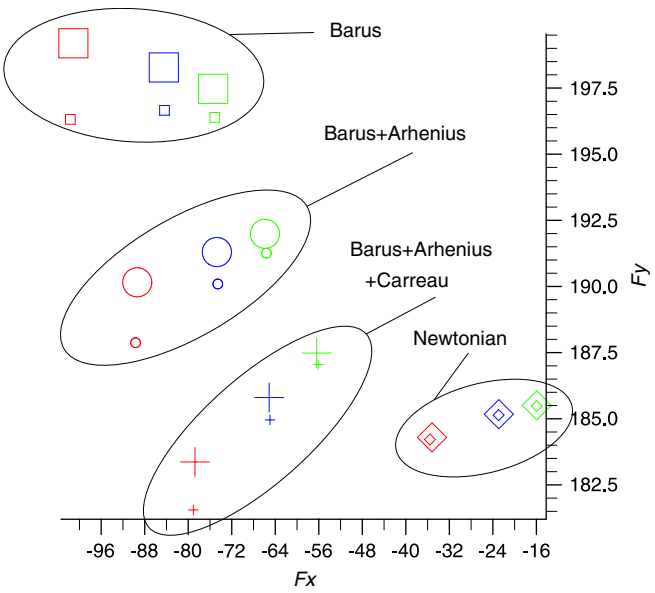

Figure 6. The load-bearing capacities for a range of models at eccentricity ratio $\varepsilon=0.8$, where we assume that the point of application is at the centre of the journal located at the origin. F_x, F_y is the force/unit length in units of $\rho R_J^3\omega^2=25\,000\,\mathrm{N\,m^{-1}}$, so that the forces shown are of the order of $10^6\,\mathrm{N\,m^{-1}}$. The squares, circles, crosses and diamonds correspond to the Barus, Barus+Arrhenius, Barus+Arrhenius+Cross and Newtonian models, respectively. The lower sound speeds increase the component of force away from the narrow gap in the x-direction. The smaller symbols are for a constant sound speed model (or $m=1$ in the Tait equation).

Table III. The value of the stability factor, χ, for a range of models and sound speeds at eccentricity ratio $\varepsilon=0.8$.

Viscosity model	$c_0=40$	$c_0=50$	$c_0=60$
Constant kinematic	0.19	0.12	0.09
Barus	0.51	0.43	0.38
Barus+Arrhenius	0.48	0.41	0.35
Barus+Arrhenius+Cross	0.45	0.38	0.31

The results suggest that increased compressibility (lower speed of sound) improves stability. A typical lubricant will have speed of sound $c_0=60R_J\omega=1500\,\mathrm{m\,s^{-1}}$.

results show that pressure is affected by sound speed and suggest that an incompressible model will exhibit a reduced range of pressure. The lack of perfect asymmetry about the narrow gap is responsible for the beneficial x component of the force away from the narrow gap.

The value $p=0$ is the actual zero pressure and not atmospheric pressure which is at a value of $p_a=0.2\rho R_J^2\omega^2=10^5\,\mathrm{Pa}\equiv 1\,\mathrm{Bar}$. However, at the values shown in Figure 7 it is a reasonable approximation to take $p_a\approx 0$ and model the onset of cavitation by assuming the cavitation region to exist in the region where $p<0$. The effect of cavitation can be modelled as a single phase

DOI: 10.1002/fld

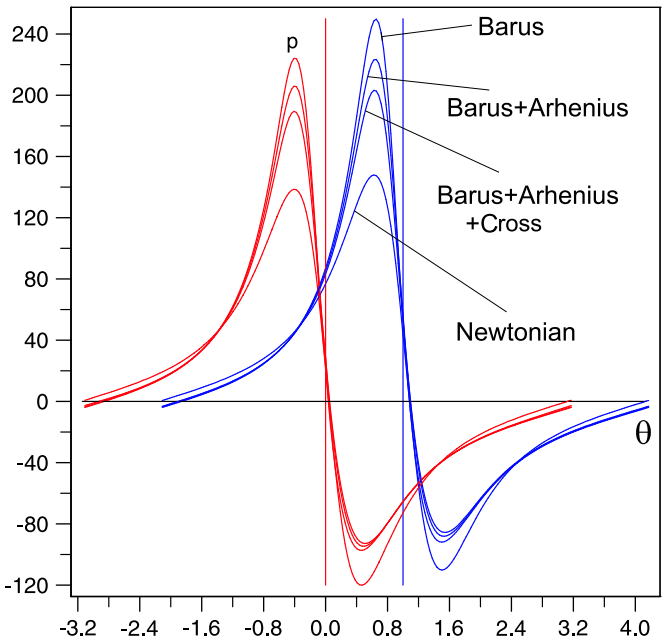

Figure 7. Pressure on the journal (the narrow gap is at $\theta=0$) in units of $\rho_0\omega^2 R_J^2 \approx 2.5\,\mathrm{Bar}$. Plots on the left (in red in the electronic version) are for $c_0=60R_J\omega$; on the right (in blue in the electronic version) $c_0=40R_J\omega$. The narrow gap is located, respectively, by the red and blue vertical lines, i.e. the two plots for the two sound speeds are displaced for ease of comparison.

fluid by assuming zero or near zero viscosity in this region, (see [7], where this is explored). However, Williams and Williams [22] show that a lubricant has a variable critical tensile strength (or negative pressure) before the liquid ruptures. This is shown to be in the region of 38 Bar, which in our units is of the order $-38\,\mathrm{Bar}=-38p_a=-7.6$. Figure 8 shows the cavitation region for a Barus–Arrhenius–Cross–Tait model for $c_0=1500\,\mathrm{m\,s^{-1}}$ and $\varepsilon=0.8$. Naturally, as the tensile strength of the liquid decreases, say due to higher temperatures, this region gets larger.

Figure 9 shows that difference in the pressure profile on the journal, although affected by sound speed, is only slight ($\sim 0.5\%$) as c_0 increases beyond $c_0=1500\,\mathrm{m\,s^{-1}}$ and suggests that an incompressible model should give comparable, but not identical, results. This is in contrast to the incompressible Navier–Stokes, which exhibits a markedly different pressure field to that of the compressible Navier–Stokes.

Figure 10 shows the effect of varying eccentricity ratio, ε, on the force on the journal for the full model for sound speed $c_0=1250\,\mathrm{m\,s^{-1}}$. The force increases with ε not only in magnitude but also in χ (Table III). Thus, the stabilizing force improves with ε. The curve shown in Figure 10 is fitted and is given by

$$F_x = 93.0\sqrt{\frac{\varepsilon}{1-\varepsilon}}$$
$$F_y = 0.008\frac{\varepsilon}{-1+\varepsilon} - 6.488\frac{\varepsilon^2}{(-1+\varepsilon)^2} - 1.236\frac{\varepsilon^3}{(-1+\varepsilon)^3} - 0.162\frac{\varepsilon^4}{(-1+\varepsilon)^4} \tag{44}$$

DOI: 10.1002/fld

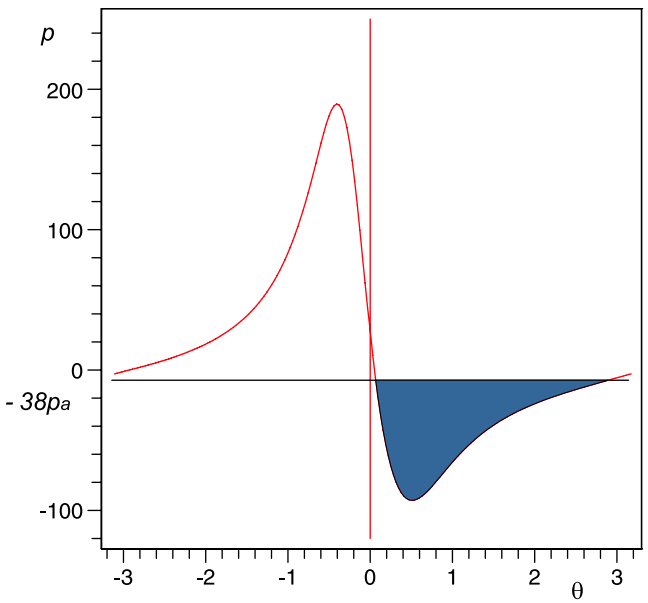

Figure 8. Pressure on the journal about the narrow gap for the full model for $c_0 = 1500\,\mathrm{m\,s^{-1}}$. The shaded region indicates where pressure falls below the cavitation pressure, -38 Bar. For stronger materials this region becomes smaller. Higher temperature weakens the fluid and, in practice, the critical cavitation pressure, p_c, can be much nearer $p = 0$.

8. THE INFLUENCE OF CENTRE OF MASS MOTION ON THE FORCE ON THE JOURNAL BEARING

We are interested in the force on the journal as its centre of mass moves in a circular path about the centre of the bearing. This is of interest for issues of both journal-bearing stability and to allow computation of the force on the journal depending on the velocity (as well as the position) of its centre of mass. Compute the position and velocity of the centre of mass of the journal at any time is usually achieved by computing the force on the journal at every time step (see, for example [5]). An alternative is to evaluate the force on the journal for all positions and velocities of the journal centre so that the evolution of the free journal's motion is then integrated as a particle of mass M_J in time using Newton's second law. The extra cost involved in this approach is the requirement of full knowledge of $\mathbf{F}$ as a function of three variables $r, \dot{\theta}, \dot{r}$ (although not θ because of symmetry). It is probably safe to neglect $\dot{r}$ and fit the two surfaces (both components of force) to a discrete set of results in the manner of equation (44), making such an approach viable. Once this force field is known, many simulations can be quickly computed in a variety of dynamically loaded scenarios. In this section we search for 'equilibrium' points in the sense that the force in the azimuthal direction (the F_y force illustrated in Figure 10) vanishes at certain rotation speeds, ω_{CM}, of the journal's centre of mass about the centre of the bearing. The critical value of ω_{CM} is seen to be approximately half that of the journal's spin, ω (half speed whirl). At this critical value, the radial component is found to be near zero, but is positive and suggests that the journal is unstable (for $c_0 = 1500\,\mathrm{m\,s^{-1}}$). This provides a more definitive measure of the stability of the

DOI: 10.1002/fld

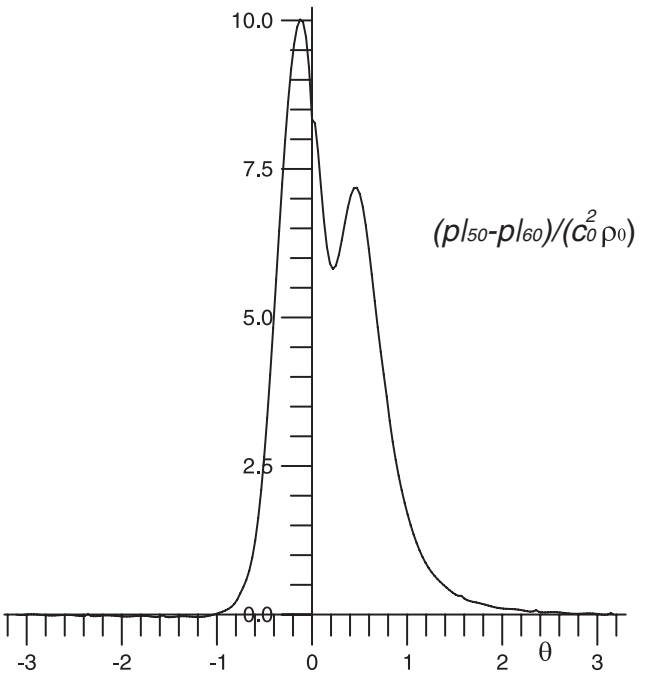

Figure 9. The pressure difference $(p|_{50} - p|_{60})/(c_0^2\rho_0)$ on the journal surface, for the Barus–Arrhenius–Cross model.

journal bearing than the χ parameter used in the previous section and may be used to effectively compare the stability of different models for fluid within the journal bearing.

We introduce a moving frame so that, for a given eccentricity ratio ε, and angle $\phi(t) = \omega_{CM} t$, the grid is that shown in Figure 5. In a rigid rotation frame, the equation of motion for the relative velocity $\mathbf{u}^*$ is

$$\frac{\mathrm{D}\mathbf{u}^*}{\mathrm{D}t} + 2\boldsymbol{\omega} \times \mathbf{u}^* + \boldsymbol{\omega} \times (\boldsymbol{\omega} \times \mathbf{x}) = -\nabla p + \nabla \cdot \mathbf{S} \tag{45}$$

where, $\boldsymbol{\omega} = \omega_{CM}\mathbf{k}$. The constitutive relations, being spatial derivatives only, are unchanged, e.g. $\nabla \mathbf{u} \to \nabla \mathbf{u}^*$. The two pseudo-forces appearing on the left-hand side are known as the Coriolis and centrifugal force, respectively. The material derivative of q can be expressed as

$$\frac{\mathrm{D}q}{\mathrm{D}t} = \left.\frac{\partial q}{\partial t}\right|_{\text{space}} + (\mathbf{u}^* + \boldsymbol{\omega} \times \mathbf{x}) \cdot \nabla q = \left.\frac{\partial q}{\partial t}\right|_{\text{rot}} + \mathbf{u}^* \cdot \nabla q$$

hence, the mass conservation is effectively unaltered in the form

$$\left.\frac{\partial q}{\partial t}\right|_{\text{rot}} + \mathbf{u}^* \cdot \nabla q = \nabla \cdot \mathbf{u}^* \tag{46}$$

and similarly with the energy conservation equations.

DOI: 10.1002/fld

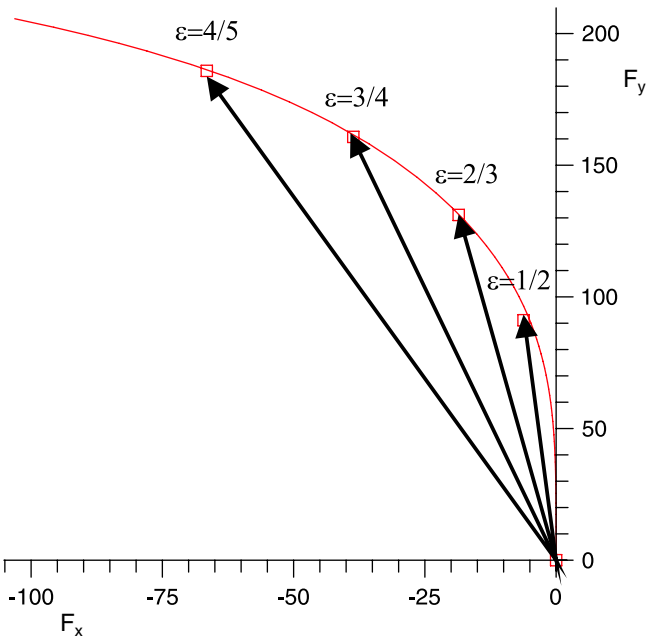

Figure 10. Force/unit length in units of $\rho R_J^3\omega^2 = 25\,000\,\mathrm{N\,m^{-1}}$ on the journal for the full Tait+Barus+Arrhenius+Cross model with speed of sound $c_0 = 50R_J\omega = 1250\,\mathrm{m\,s^{-1}}$ for different eccentricity ratios ε.

In two dimensions, with the rotation of the plane about the normal to the plane, $\boldsymbol{\omega} = \omega_{CM}\mathbf{k}$, (45) becomes

$$\frac{\mathrm{D}\mathbf{u}^*}{\mathrm{D}t} + 2\omega\mathbf{k}\times\mathbf{u}^* + \omega^2\mathbf{x} = -\nabla p + \nabla\cdot\mathbf{S} \tag{47}$$

where the position, $\mathbf{x}$, and operator ∇ all refer to the coordinates moving with the rotating frame. The semi-Lagrangian treatment of the convection term as explained in detail in [1] is modified only to the extent that the relative velocity, $\mathbf{u}^*$, is used instead of $\mathbf{u}$ to find the previous particle position from its current position at a GLL point. This implies, for example, that a particle stationary in the moving frame at a point, p, contributes $\mathrm{D}\mathbf{u}^*/\mathrm{D}t|_p = \mathbf{0}$. However, there is an option here to merge the Coriolis and centrifugal forces into a modified semi-Lagrangian method.

The discretization of the new term $2\omega\mathbf{k}\times\mathbf{u}^*$ alters (34) by

$$\bar{\bar{M}}^{ab} \to \bar{\bar{M}}^{ab} + 2\omega\varepsilon^{ab}\bar{\bar{A}}$$

Unfortunately, this destroys the symmetry of the discrete operator and hence we incorporate the Coriolis term explicitly. Thus, the right side of (33) given by (35) is altered by

$$\bar{v}^b \to \bar{v}^b - \Delta t\,(2\omega\varepsilon^{ab}\bar{u}_a^n\cdot\bar{\bar{A}} + \omega^2\bar{x}^b\cdot\bar{\bar{A}})$$

where $\bar{x}^b$ holds the positions of the GLL points and ε^{ab} is the alternating tensor.

DOI: 10.1002/fld

Table IV. Table of values showing the outward radial force/unit length in units of $\rho R_J^3 \omega^2 = 25000\,\mathrm{N\,m^{-1}}$ on a journal when the journal centre rotates about the centre of the bearing at $\omega \approx 0.514\omega$ at different eccentricity ratios, ε.

ε	ω	F_{radial}, $c = 1500\,\mathrm{m\,s^{-1}}$	F_{radial}, $c = 1000\,\mathrm{m\,s^{-1}}$
1/2	0.5141	0.104	0.117
2/3	0.5142	0.130	0.145
3/4	0.5142	0.155	0.170
4/5	0.5142	0.178	0.191
5/6	0.5142	0.199	0.212
6/7	0.5142	0.219	0.234
7/8	0.5143	0.245	0.258
8/9	0.5143	0.267	0.284
9/10	0.5143	0.290	0.313

The value of ω is shown for $c = 1500\,\mathrm{m\,s^{-1}}$ but is effectively unchanged for the lower value of $c_0 = 1000\,\mathrm{m\,s^{-1}}$. The result shows that a free journal will spiral out and stability is not improved by a lower speed of sound.

8.1. Half speed whirl

It is well known that a freely rotating journal within a bearing undergoes what is known as 'half speed whirl'. This is a phenomenon whereby the centre of mass of the journal rotates at a frequency, ω_{CM}, half that of its spin, ω. The suggestion that whirl instability occurs in the dynamically loaded journal with zero applied load has been made by many investigators and a journal that exhibits this effect is deemed to have failed. Full cavitation modelling is expected to mitigate this effect by damping out the self-excited instability. We can investigate this effect by looking for frequencies, ω, where the azimuthal force falls to zero. Using a simple bisection method, we find that the critical angular velocity, ω, is approximately 0.514ω for a range of eccentricities, ε. The model used is the full Tait–Barus–Arrhenius–Cross model and the results suggest that a free (i.e. unloaded) journal is unstable and spirals outwards indefinitely. Table IV gives that the values obtained for the radial force indicate that the outward force increases with eccentricity, with the angular velocity remaining approximately constant. The appearance of the vortex is substantially altered (see Figure 11) by the rotation. Other field variables behave quite differently, e.g. both $\nabla \cdot \mathbf{u}$ and $q \equiv \ln \rho$ are approximately zero, the temperature, Θ, becomes a function of the radial coordinate only and the principal stress becomes a function of the azimuthal coordinate only with reflection symmetry about the x-axis.

9. THE BEHAVIOUR OF THE FIELD VARIABLES WITHIN THE JOURNAL BEARING

Figure 11 shows the velocity field for $\varepsilon = 0.9$, which indicates a region of recirculation for both the static and rotating frames. As is usual the dimensions of the fluid domain have been exaggerated in the figures in order to explore the dynamics within the thin fluid domain. Scalar values of the true field are simply displaced by this transformation. In order to display vector quantities, one needs to find the tangent map associated with the transformation used (a display of the true field in the exaggerated domain looks unphysical and misleading). Let us define the mapping given by (26) by $\Phi_{\varepsilon,R_J} : (r, \theta) \mapsto (x, y)$ and the mapping used to display figures such as Figure 11

DOI: 10.1002/fld

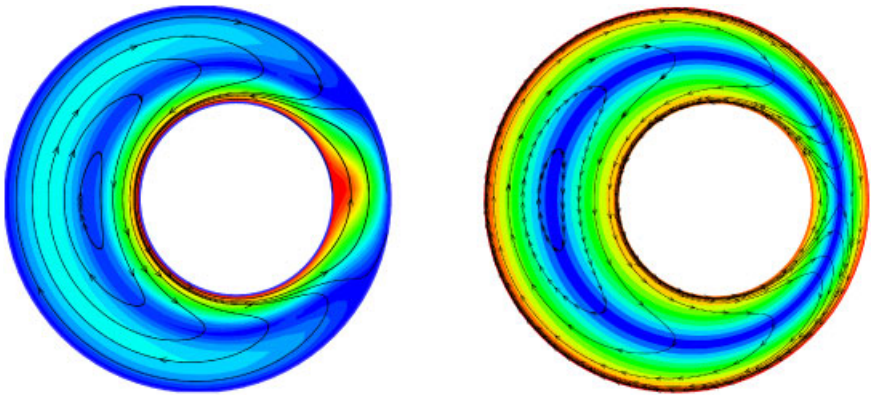

Figure 11. Streamlines and velocity magnitude for eccentricity $\varepsilon=0.9$, revealing the recirculation region where the velocity field rotates in an opposite sense to the journal. The left-hand picture is for the static journal and the right is for centre of mass rotation $\omega_{CM}=0.514\omega$. The vortex size clearly increases as $\omega_{CM}\to\omega/2$.

as $\Phi_{\varepsilon',R'_J}:(r,\theta)\mapsto(X,Y)$, where the values used for the display pictures are $\varepsilon'=0.4$, $R'_J=0.5$ (as compared with $R_J=0.999$). Then $\Phi^{-1}_{\varepsilon,R_J}\circ\Phi_{\varepsilon',R'_J}:(x,y)\mapsto(X,Y)$. This induces a linear map $\mathbf{u}'=\mathbf{u}\mathbf{A}^{-1}\mathbf{B}\mathbf{A}'$, where $\mathbf{A}$ is the matrix associated with (26):

$$\mathbf{A}=\begin{bmatrix}\cos\theta-\varepsilon & \sin\theta\\ -r\sin\theta & r\cos\theta\end{bmatrix},\quad \mathbf{B}=\begin{bmatrix}\lambda & 0\\ 0 & 1\end{bmatrix},\quad \mathbf{A}'=\begin{bmatrix}\cos\theta-\varepsilon' & \sin\theta\\ -r'\sin\theta & r'\cos\theta\end{bmatrix} \tag{48}$$

where $\lambda\equiv(1-R')/(1-R)$ and $r'=R'+\lambda(r-R)$. Figure 11 shows some streamlines against a background of velocity magnitude. The recirculation region forms more than half of the domain and may suggest a mechanism for journal-bearing efficiency in that the journal does not apparently drag round all the fluid except in the case of low eccentricity. The recirculation region can be seen to move at lower speed than the fluid closer to the journal.

For an incompressible fluid, the momentum field is of no more interest than the velocity field. However, for the compressible case we expect qualitative differences due to variable density. Figure 12 shows the magnitude of the momentum field on the left and the velocity field on the right. We note that, unlike the velocity field, there is a strong asymmetry in the magnitude of momentum field about the line through the journal and bearing centres (the x-axis).

The temperature field is shown for sound speed $c=1500\,\mathrm{m\,s^{-1}}$ in Figure 13. We note that the lower value of c creates a wider temperature distribution. The temperature effects the viscosity through the Arrhenius factor $\exp(-\beta\Theta/(\Theta+\Theta_0))$. This distribution is shown in Figure 14 and may be compared with the temperature in Figure 13, where we note that the factor is larger for lower values of temperature, Θ; hence, creating a higher viscosity area away from the narrow gap. Perhaps the most surprising observation about the temperature plots is the loss of symmetry. There are two hot areas asymmetrically distributed either side of the narrow gap and of different magnitudes. Figures 15 and 16 demonstrate that the temperature field is almost at the limiting value, $\lim_{c_0\to\infty}\Theta$, when $c_0=60R_J\omega=1500\,\mathrm{m\,s^{-1}}$. This result suggests that, for realistic values of

DOI: 10.1002/fld

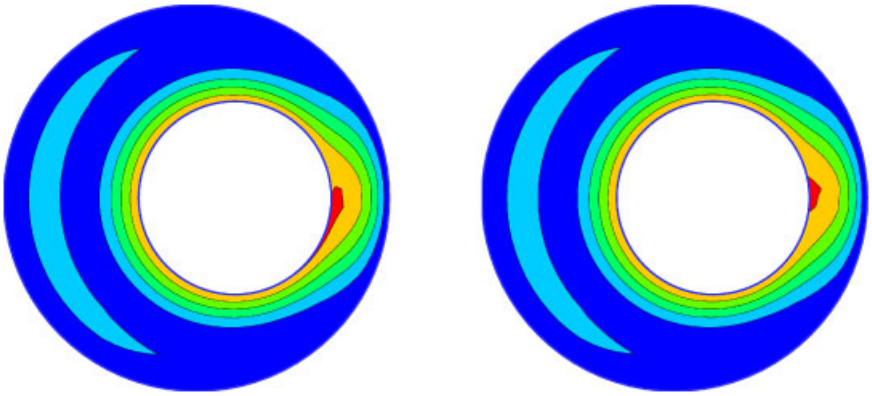

Figure 12. Magnitude of momentum $\mathbf{p}=\rho\mathbf{u}$ (left) and velocity $\mathbf{u}$ (right). The variation in density about the narrow gap brings about a loss of symmetry in the contours of momentum magnitude as compared with contours of speed. This becomes more marked at a lower speed of sound.

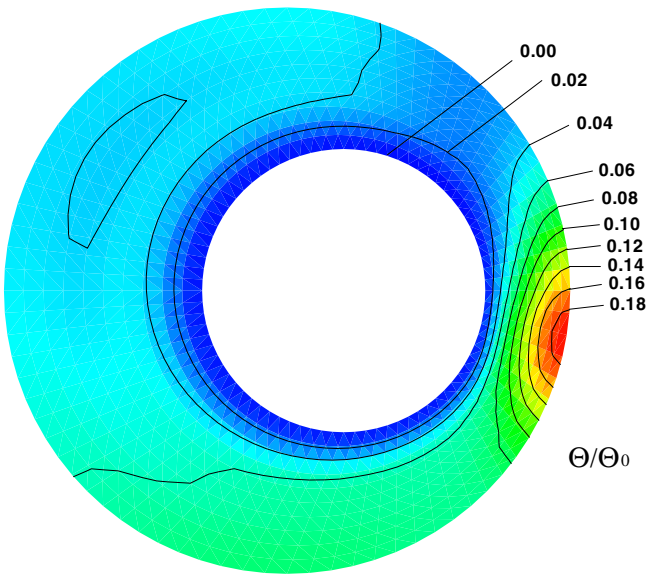

Figure 13. Contours of temperature, Θ/Θ_0 for sound speed $c_0=60R_J\omega$. The higher temperatures are found in the fluid entering the narrow gap.

c_0, the temperature field is well approximated using an incompressible model, which is common practice.

The viscosity is affected via the temperature and is shown in Figure 17 for two different values of c, where we note that there is a sharper gradient at the narrow gap for the lower value of sound speed for an otherwise similar range of other parameters.

DOI: 10.1002/fld

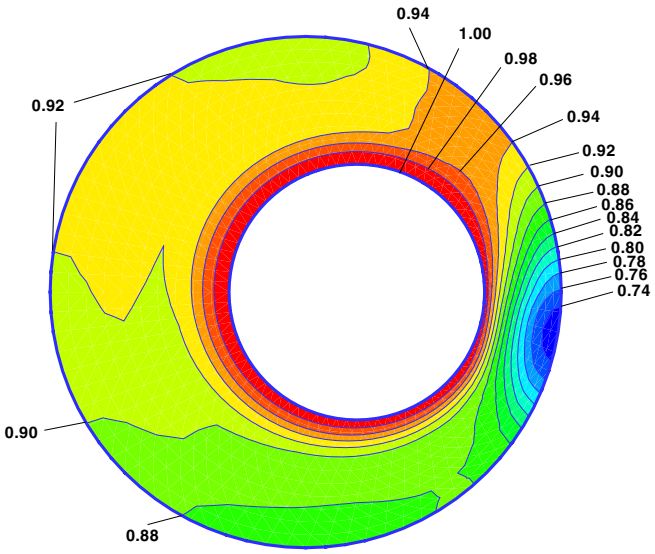

Figure 14. Contours of the Arrhenius factor, $\exp\frac{-\beta\Theta}{\Theta+\Theta_0}$, for sound speed $c_0 = 1500\,\mathrm{m\,s^{-1}}$.

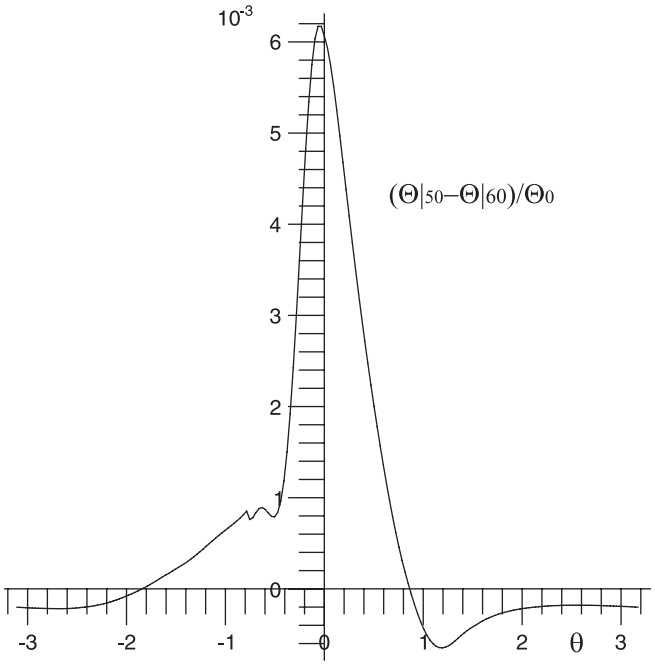

Figure 15. Temperature difference, $(\Theta|_{50} - \Theta|_{60})/\Theta_0$, for the two sound speeds $c_0 = 50 R_J \omega$ and $c_0 = 60 R_J \omega$ with the Cross model.

DOI: 10.1002/fld

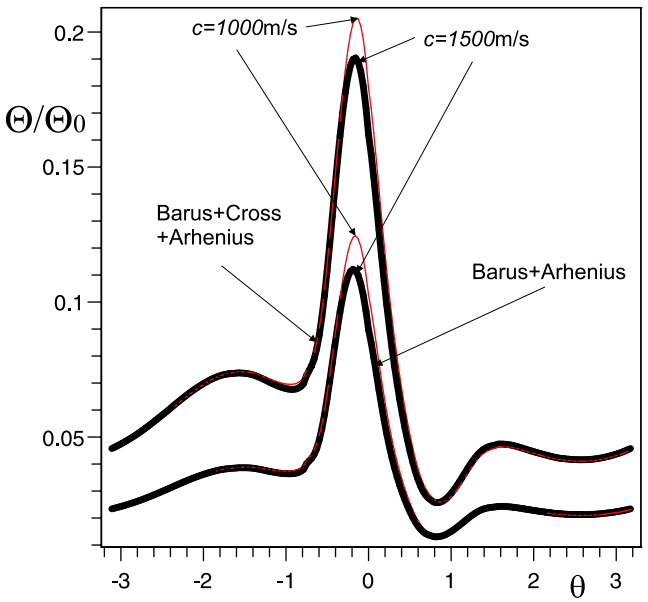

Figure 16. Temperature, Θ/Θ_0, for sound speeds $c_0 = 40 R_J \omega$ and $c_0 = 4060 R_J \omega$ on the bearing (1000 and 1500 m s^{-1}, respectively). The profiles for temperature almost coincide except for the peak value at the narrow gap, which exhibits a higher temperature for the lower speed of sound. The Cross model has a marked effect on the temperature profile, the journal-bearing fluid being at a higher temperature.

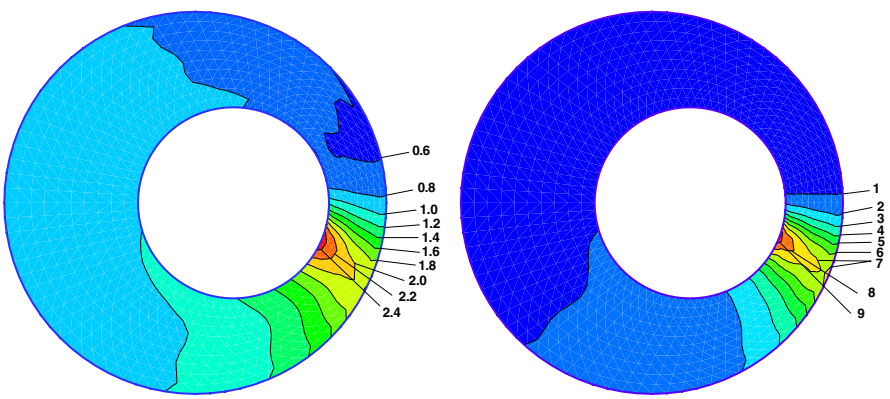

Figure 17. Contours of viscosity, η/η_0: speed of sound, $c = 1500\,\mathrm{m\,s^{-1}}$ (left), $c = 1000\,\mathrm{m\,s^{-1}}$ (right). The lower sound speed (right) generates a larger range of viscosity.

The principal stress is shown in Figure 18 for two values of speed of sound, c_0. Comparing this field with that of the velocity we note the correspondence between the area of low stress (<0.02) and where the motion of the fluid is approximately clockwise (opposite to that of the journal rotation). The area on the journal at the narrow gap is also near zero and, in fact, has a

DOI: 10.1002/fld

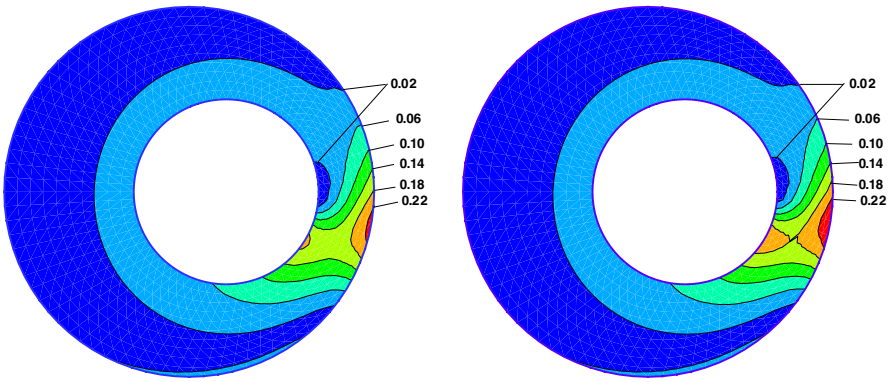

Figure 18. Contours of the principal stress: $c=1500\,\mathrm{m\,s^{-1}}$ (left), $c=1000\,\mathrm{m\,s^{-1}}$ (right).

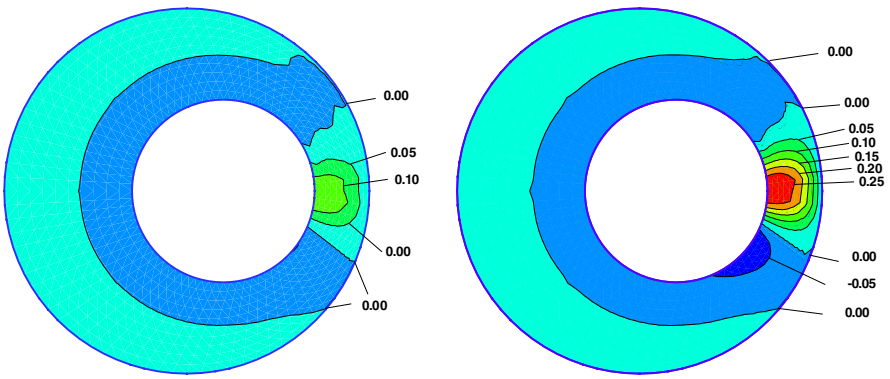

Figure 19. Contours of $\nabla\cdot\mathbf{u}$: $c=1500\,\mathrm{m\,s^{-1}}$ (left), $c=1000\,\mathrm{m\,s^{-1}}$ (right). The lower sound speed is associated with larger values for the divergence of $\mathbf{u}$.

shear stress opposite to that of the shear stress on the rest of the journal. The lower sound speed leads to a slight increase in stress levels.

It is also interesting to inspect the values of $\nabla\cdot\mathbf{u}$ for an incompressible fluid, which is shown in Figure 19. This reveals a significant difference between a fluid with $c_0=1500$ and $1000\,\mathrm{m\,s^{-1}}$. We notice in particular, a region adjoining the narrow gap where there is net volume flow *out* and another area also adjoining the journal where there is a net volume flow into the region. Now these results are for steady state and thus $\nabla\cdot(\rho\mathbf{u})=0$, which implies

$$\nabla\cdot\mathbf{u}=-\frac{1}{\rho}\nabla\rho\cdot\mathbf{u}\equiv-\nabla q\cdot\mathbf{u}$$

Hence, for regions with $\nabla\cdot\mathbf{u}>0$ the density, ρ, decreases in the direction of the flow, which in turn explains, for example, the lower pressure immediately downstream from the narrow gap.

DOI: 10.1002/fld

10. SUMMARY OF OBSERVATIONS AND FUTURE MODELLING

In this paper different aspects of a mathematical model for lubricated oils have been described. The different components of this model have been isolated to monitor their influence on load-bearing capacity. The model includes an equation of state that depends on both temperature and density, viscous heating, temperature and strain rate thinning and piezoviscosity. There is an interplay between these different aspects of the model within the journal bearing. The equation of state has limited direct impact on the dynamics because of the use of a small expansion parameter, α. Thus, the only non-negligible coupling between the energy and momentum equations is via the temperature thinning viscosity.

The model predicts instability in the free (unloaded) journal. This instability would be inhibited by the application of a uni-directional load because the journal is then not able to exhibit whirling. On the other hand, this result suggests that an oscillatory load could not be sustained by such a model fluid without breaking down.

We have avoided cavitation modelling at this stage, which will be a major feature in subsequent papers, in order to study what effects the model exhibits (if any) by the combination of compressibility with a generalized Newtonian model. In particular, it is observed that for values of $c_0 > 1500\,\mathrm{m\,s^{-1}}$, the temperature and pressure profiles do not significantly change. The implication here is that many of the properties of the lubricant are adequately captured by an incompressible model. However, for values of $c < 1250\,\mathrm{m\,s^{-1}}$ the model begins to show differences that indicate the importance of the role of compressibility in cavitation modelling, which is essential to realistic lubricant modelling due to the stresses present in typical journal-bearing operation.

ACKNOWLEDGEMENTS

The authors would like to acknowledge the financial support of the EPSRC (Engineering and Physical Sciences Research Council) of the United Kingdom through grant EP/C513037.

REFERENCES

1. Bollada P, Phillips TN. On the effects of an isothermal compressible viscous lubricant on the load-bearing capacity of a journal bearing. *International Journal for Numerical Methods in Fluids* 2007; **55**(11):1091–1120.
2. Tait PG. *Physics and Chemistry of the Voyage of H.M.S. Challenger*, vol. 2/4. HMSO: London, 1888.
3. Phan-Thien N. *Understanding Viscoelasticity*. Springer: Berlin, 2002.
4. Davies AR, Li XK. Numerical modelling of pressure and temperature effects in viscoelastic flow between eccentrically rotating cylinders. *Journal of Non-Newtonian Fluid Mechanics* 1994; **54**:331–350.
5. Li XK, Davies AR, Phillips TN. A transient thermal analysis for dynamically loaded bearings. *Computers and Fluids* 2000; **29**:749–790.
6. Gwynllyw DRh, Davies AR, Phillips TN. A moving spectral element approach to the dynamically loaded journal bearing problem. *Journal of Computational Physics* 1996; **123**:476–494.
7. Gwynllyw DRh, Davies AR, Phillips TN. On the effects of a piezoviscous lubricant on the dynamics of a journal bearing. *Journal of Rheology* 1996; **40**:1239–1266.
8. Gwynllyw DRh, Phillips TN. Preconditioned iterative methods for unsteady non-Newtonian flow between eccentrically rotating cylinders. *SIAM Journal on Scientific Computing* 1996; **17**:1369–1394.
9. Phillips TN, Need RE, Davies AR, Williamson B, Scales LE. The effect of viscoelasticity on the performance of dynamically loaded journal bearings. *Technical Report 982639*, Society of Automotive Engineers, 1998.
10. Dymond JH, Malhotra R. The tait equation 100 years on. *International Journal of Thermophysics* 1988; **9**:941–950.
11. Kirkwood JG, Bethe H. The pressure wave produced by an underwater explosion, pt. I. *Technical Report 588*, 1942.

DOI: 10.1002/fld

12. Keshtiban IJ, Belblidia F, Webster MF. Computation of incompressible and weakly-compressible viscoelastic liquids flow: finite element/volume schemes. *Journal of Non-Newtonian Fluid Mechanics* 2005; **126**:123–143.
13. Belblidia F, Keshtiban IJ, Webster MF. Stabilised computations for viscoelastic flows under compressible implementations. *Journal of Non-Newtonian Fluid Mechanics* 2006; **134**:56–76.
14. Keshtiban IJ, Belblidia F, Webster MF. Numerical simulation of compressible viscoelastic liquids. *Journal of Non-Newtonian Fluid Mechanics* 2004; **122**:131–146.
15. Woods LC. The thermodynamics of fluid systems. *Oxford Engineering*, *Science Series 2*, 1986.
16. Bird RB, Stewart WE, Lightfoot EN. *Transport Phenomena*. Wiley: New York, 2002.
17. Hosangadi A, Ahuja V, Arunajatesan S. A generalized compressible cavitation model. *CAV 2001*: *Fourth International Symposium on Cavitation*, June 20–23, California, Institute of Technology, Pasadena, CA U.S.A., 2001.
18. Gad el Hak M. Questions in fluid mechanics: Stokes hypothesis for a Newtonian, isotropic fluid. *Journal of Fluids Engineering* 1995; **117**:3–5.
19. Houpert LG, Hamrock BJ. New results of traction force calculations in elastodynamic contacts. *Journal of Tribology—Transactions of the ASME* 1985; **107**:241–248.
20. Houpert LG, Hamrock BJ. Fast approach for calculating film thicknesses and pressures in elastohydrodynamically lubricated contacts at high loads. *NASA STI/Recon Technical Report N*, vol. 85, 1985; 30242.
21. Gwynllyw DRh, Phillips TN. Some issues regarding spectral element meshes for moving journal bearing systems. *International Journal for Numerical Methods in Fluids* 2005; **48**:423–454.
22. Williams PR, Williams RL. Cavitation properties of oils under dynamic stressing by tension. *Journal of Fluids Engineering* 2005; **127**(2):282–289.

DOI: 10.1002/fld